SUPPLEMENTARY INFORMATION

for

Self-Propelled MOF Micromotors: A Smart Solution for Antibiotic Pollution and Resistance Control

Rashi Bhardwaj*[1], Karan Hadwani[1], Jay Singh[2], Kuntal Manna[3], Deepika Chauhan[1] Tinku Basu[1]

[1]Amity Centre for Nanomedicine, Amity University Uttar Pradesh; [2] Department of Chemistry, Institute of Science, BHU Varanasi, [3] IIT Delhi

Corresponding Author Email: rashii.sharma94@gmail.com ; Phone No. +91-9582196955

TABLE OF CONTENTS

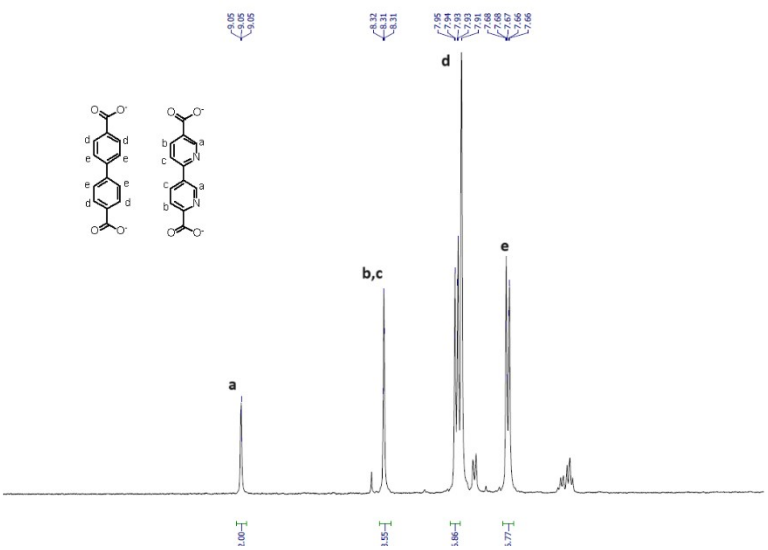

SI 1 NMR analysis of both Bidentate Zr UiO MOF and Fe Zr UiO MOF MM

Figure S 1 NMR analysis of Bidentate Zr UiO MOF and Fe Zr UiO MOF MM respectively

SI 2 HPLC analysis of amoxicillin antibiotic

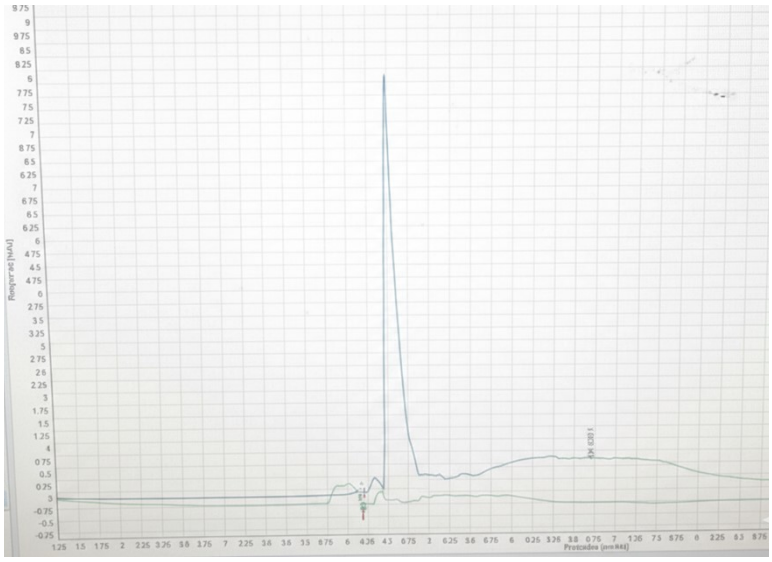

Figure S 2 HPLC analysis of pure (dark blue) and residual (light blue) antibiotic

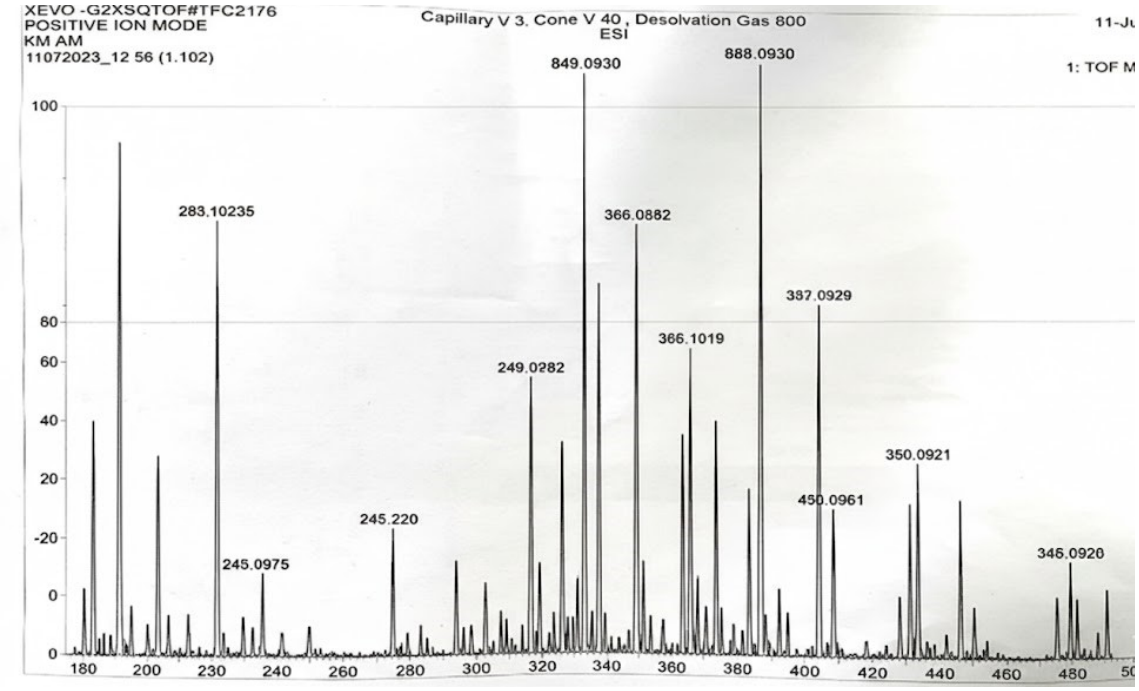

Figure S 3 HRMS analysis of the obtained residual amoxicillin antibiotic

SI 3

HRMS analysis of degraded amoxicillin antibiotic

SI 4 XPS analysis of Fe Zr MOF MM after degradation

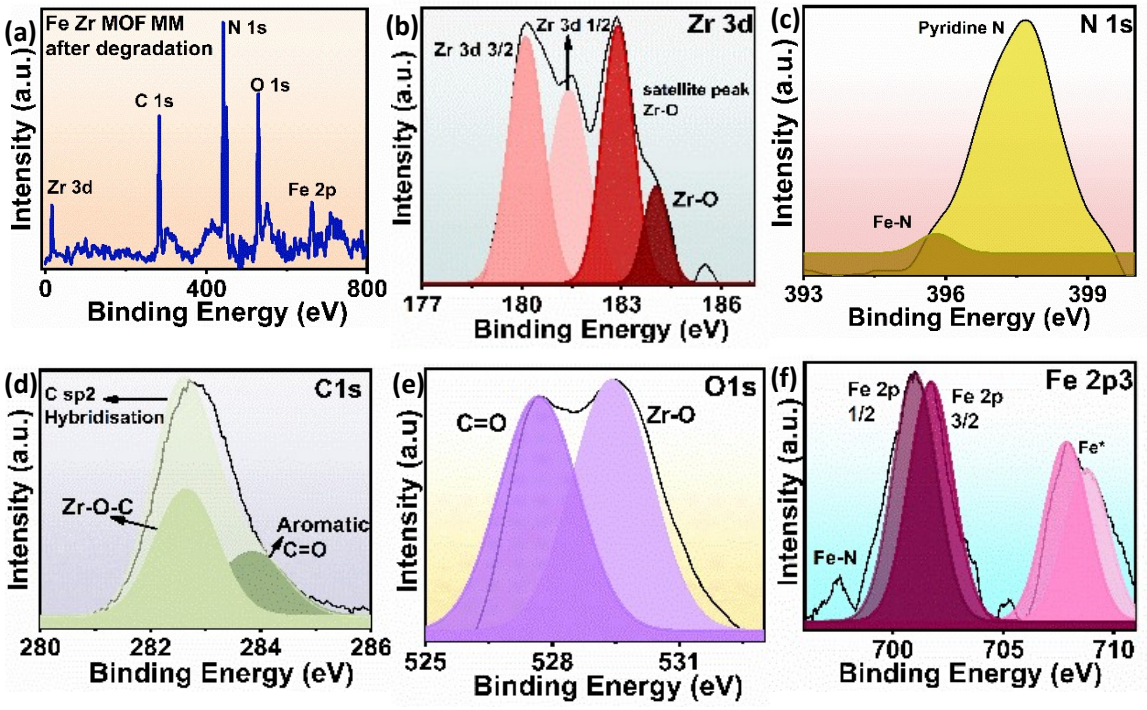

Figure S 4 XPS analysis graph of (a) the survey plot, (b) Zr 3d (c) N 1s orbital (d)O 1s orbital and (e) C 1s orbital and (f) Fe 2p3 orbital plot of Fe Zr MOF MM after degradation respectively.

Figure S4 represents the complete XPS spectral analysis of (a) the survey plot, (b) Zr 3d (c) N 1s orbital (d)O 1s orbital and (e) C 1s orbital and (f) Fe 2p3 orbital plot of Fe Zr MOF MM after it was interacted with amoxicillin antibiotic. Fig.S3 (a) shows the presence of all elements namely Zr, C, N, O and Fe in the full spectral graph for full range confirming that material has not degraded or broken down when interacted with amoxicillin antibiotic in presence of fuel. Moving on to individual elements, For Zr (Figure. S3c), the spectra disclose 4 peaks for Zr 3d 3/2, Zr 3d ½, a satellite peak for Zr-O linkage and Zr-O linkage at 180.2eV, 181.4eV, 182.9eV and 184.05eV respectively. It can be noted that the peak matches with what are observed when XPS analysis was done before degradation. For example, in the N in Figure S3(d), two peaks are noted at 395.8 and 397.71eV for satellite peak of pyridine N and pyridinic N itself. For C 1s in Figure S3e three peaks are distinguished for Zr-O-C linkage at 282.42eV, C Sp2 hybridisation at 283.05eV and aromatic C=O linkage at 284.1eV, respectively. Two peaks same as before are noted in O1s (figure S3e) for Zr=O linkage at 529.7eV and O* at 527.52eV which again can be due to the fact that the O is bonded to no metallic elements like Carbon which is possible in this case or there may be some defects present in the MOF structural network. For Fe 2p3 orbital (figure S3f) 4 peaks at 697.5eV, 700.9eV,701.87eV and 708.30 eV are ascribed for Fe-N linkage, Fe 2p ½ and Fe 2p 3/2. Interestingly, the XPS spectrum of Fe reveals a peak at 708.30 eV, which is assigned to the Fe 2p3/2 satellite peak of iron atoms in a high oxidation state and bonded to pyridine ligands.

SI 5 Stability and Reusability Study of Fe Zr MOF MM

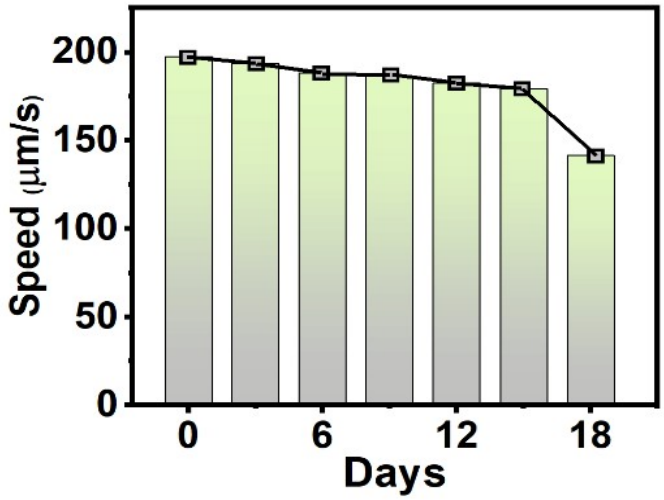

Figure S 5 stability study in terms of speed of Fe Zr MOF MM

Figure S5 represents the stability study in terms of speed of Fe Zr MOF MM. The stability of Fe Zr MOF MM was checked in water to ascertain that the material can degrade the antibiotic in water without breaking itself down. A certain weight (20mg) of Fe Zr MOF MM was soaked in water to check to aqueous stability of the developed Fe Zr MOF MM and testing was conducted every 3 days, 2mg of material was taken out and dried and movement was checked with optimized fuel, and MSA concentration till a drastic decrease in speed was noted (Figure 3d). It was noted that till 15th day, the decrease in speed is very nominal i.e., 180μm/s (less than 10% decrement) but on 18th day the speed decreased drastically from

197µm/s to 140µm/s (30% decrease in speed). A very sluggish bubble generation was noted as well. It may be inferred that the prolong exposure of Fe Zr MOF MM in water in the presence of fuel may cause breaking of the bonds formed between Fe with N present in the pyridine

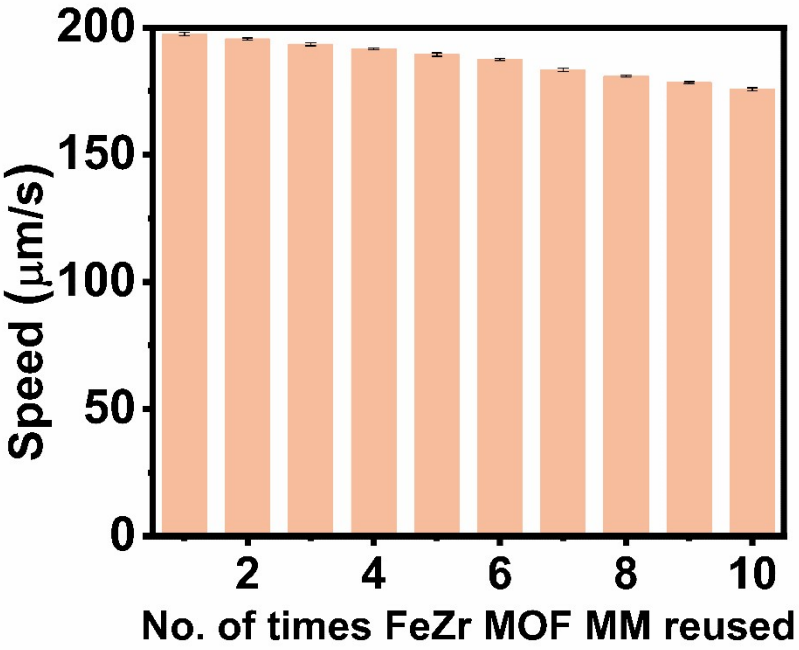

Figure S 6 the reusability graph of Fe Zr MOF MM as a plot of usage vs speed in µm/s

The operational stability and reusability of the Fe-Zr MOF MMs were evaluated over ten consecutive catalytic cycles. Following each cycle, the MMs were recovered, rinsed with deionized water, and vacuum-dried before reuse in the degradation of amoxicillin. As illustrated in Figure S5, the micromotors exhibited robust mechanical and catalytic durability; the average speed transitioned from 197.2 µm/s in the first cycle to 175.69 µm/s by the tenth cycle. This marginal 11% reduction in velocity confirms the excellent reusability and structural integrity of the Fe-Zr MOF MM platform for long-term environmental remediation applications.

SI 6 Recyclability Studies of Fe Zr MOF MM

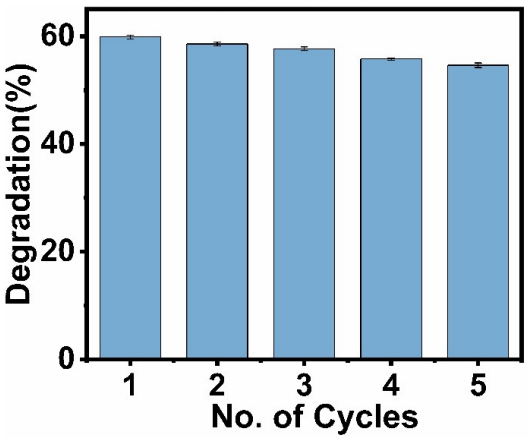

Figure S 7 recyclability test of Fe Zr MOF MM as a plot of No. of Cycles vs degradation %

Figure S 7 represents the recyclability test of Fe Zr MOF MM as a plot of No. of cycles vs degradation efficiency in %. Following each cycle, the MMs were recovered, rinsed with deionized water, and vacuum-dried before reuse in the degradation of amoxicillin. Fe Zr MOF MM displayed excellent catalytic activity for up to 5 cycles with only 10% reduction in the catalytic efficiency going from 59.6% to 54.7% after 5 cycles.

SI 7 Zeta Potential Studies

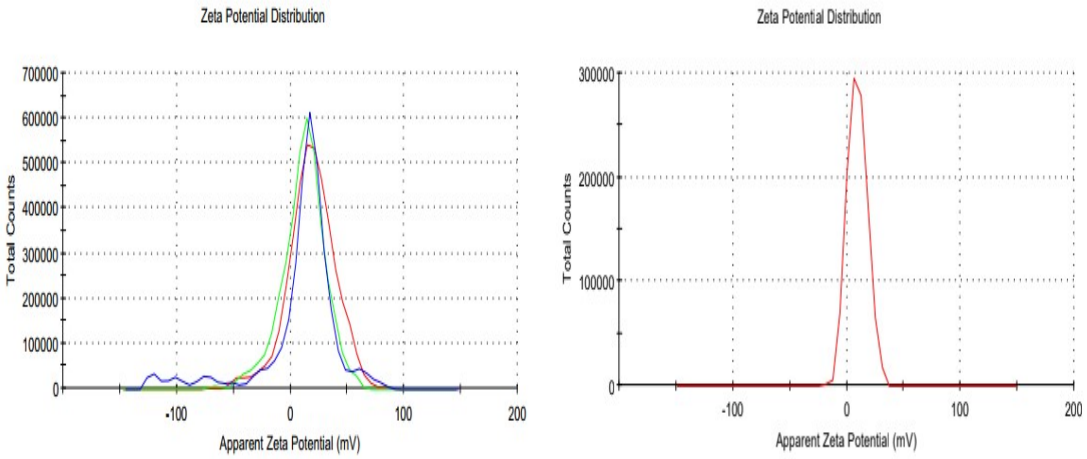

Figure S8 Zeta potential analysis of FE Zr MOF MM (a) before (b) after the catalytic reaction

SI 8 Porosity & Surface Area analysis

SI 8.1 BET Analysis

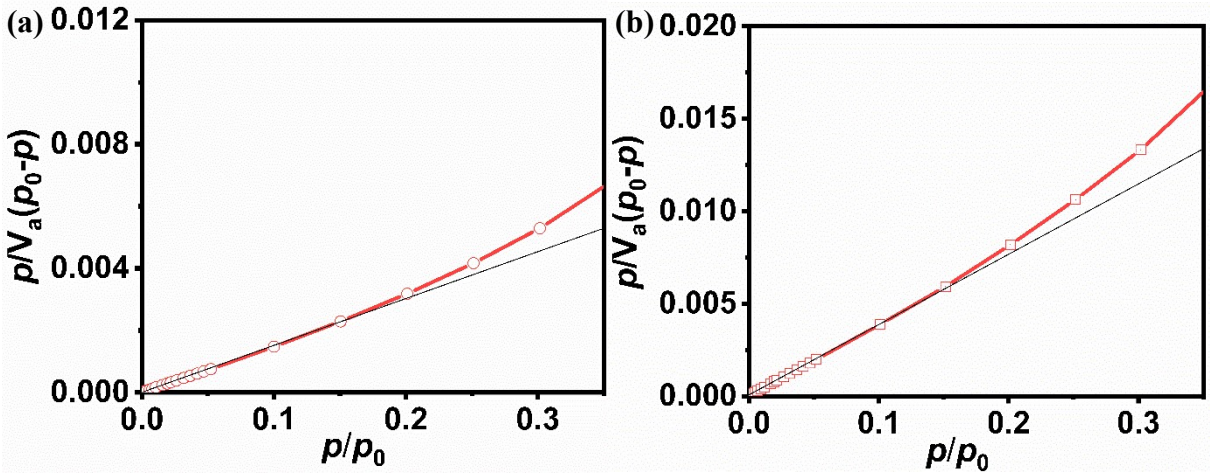

Figure S9 BET analysis of (a) bidentate Zr UiO MOF (b) Fe Zr MOF MM respectively

The corresponding BET surface area analysis in Figure S9 (a&b) reveals significant changes in the textural properties of the bidentate Zr UiO MOF upon post-synthetic

metalation with Fe to form Fe Zr MOF MM. The parent Bidentate Zr UiO MOF exhibits a high BET specific surface area of 308.80 m^2g^{-1} with a total pore volume of 0.2987 cm^3g^{-1}. Following the incorporation of Iron to form the Fe Zr MOF MM, a substantial decrease in surface area to 117.87 m^2g^{-1} (~61.8% reduction) and a decrease in total pore volume to 0.2197 cm^3g^{-1} are observed.

Table S1: summarising all parameter wise data obtained for Zr UiO bidentate MOF and Fe Zr MOF MM for BET analysis

S.No.	Parameter	Bidentate Zr UiO MOF	Fe Zr MOF MM
1.	BET Surface Area (a_s,BET)	308.80 m^2g^{-1}	117.87 m^2g^{-1}
2.	Total Pore Volume (V_p)	0.2987 cm^3g^{-1}	0.2197 cm^3g^{-1}
3.	Monolayer Capacity (V_m)	70.948 cm^3g^{-1}	27.081cm^3g^{-1}
4.	Average Pore Diameter	3.87 nm	7.46 nm

This pronounced reduction in surface area, alongside the decrease in the monolayer adsorption capacity from 70.948 cm^3g^{-1} to 27.081 cm^3g^{-1}, suggests that the Fe complexes are successfully coordinated to the pyridine groups within the framework's internal cavities rather than merely residing on the external crystal surface. Furthermore, the average pore diameter increases from 3.87 nm in bidentate Zr UiO MOF to 7.46 nm in Fe Zr MOF MM. This apparent increase in average diameter is attributed to the selective filling or blockage of the smaller micropores by the Fe species, which causes the remaining accessible porosity to be dominated by larger mesoporous/interparticle voids. Collectively, these BET parameters demonstrate that Fe loading predominantly affects the microporous environment of the bidentate framework, confirming successful site-specific metalation.

SI 8.2 N_2 Adsorption & desorption Isotherm

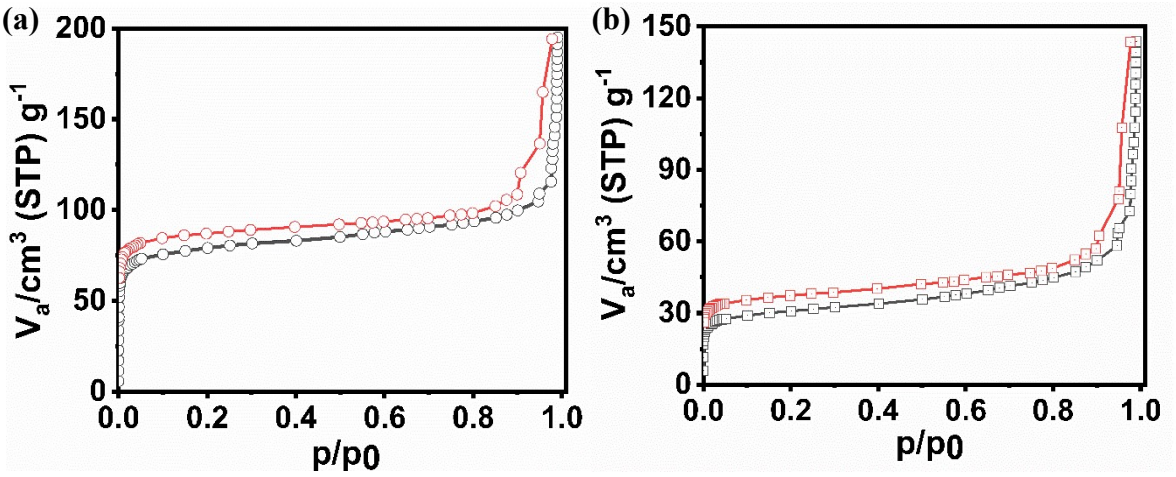

Figure S10 N_2 Adsorption Desorption Isotherm analysis of (a) bidentate Zr UiO MOF (b) Fe Zr MOF MM respectively

The full N_2 adsorption–desorption isotherms for both the parent bidentate Zr UiO MOF and the Fe Zr MOF MM have been provided (Figure S10). Both samples exhibit Type IV isotherms

with H3/H4 hysteresis loops, characteristic of materials containing both micropores (from the UiO framework) and mesoporous/macroporous voids (likely interparticle porosity). The post-synthetic metalation with Fe significantly impacts the overall porosity, though the fundamental pore structure remains intact.

Table S2: table containing all features and their respective values for both Zr UiO bidentate MOF and Fe Zr MOF MM using N_2 Adsorption and desorption isotherm.

S.No.	**Feature**	**Bidentate Zr UiO MOF**	**Fe Zr MOF MM**
1.	Micropore Uptake ($p/p_0<0.1$)	~80 cm^3/g	~35 cm^3/g
2.	Mesopore Plateau ($0.1<p/p_0<0.8$)	Gradual rise: 80 to 100 cm^3/g	Gradual rise: 35 to 50 cm^3/g
3.	Macropore/Interparticle ($p/p_0>0.9$)	Steep rise to ~195 cm^3/g	Steep rise to ~145 cm^3/g
4.	Hysteresis Loop	Present, Type H4/H3	Present, Type H4/H3

- Microporosity**:** Upon Fe loading, there is a substantial decrease in nitrogen uptake at low relative pressures ($p/p_0 < 0.1$). The volume adsorbed drops from approximately 80 cm^3/g in the parent bidentate Zr UiO MOF to approximately 35 cm^3/g in the Fe-loaded version i.e., Fe Zr MOF MM. This suggests that the Fe species are successfully coordinated to the pyridine groups within the microporous channels of the bpydc linkers, effectively 'occupying' or partially blocking the micropore volume.
- Mesoporosity/Macro porosity: The total pore volume at high relative pressures ($p/p_0 \rightarrow 1.0$) also decreases from ~195 cm^3/g to ~145 cm^3/g. While the general shape of the mesoporous uptake remains similar, the overall reduction indicates that Fe loading occurs in the porous network.

Henceforth it was concluded that Fe loading predominantly impacts the microporosity by occupying the space within the framework cages where the bpydc sites are located. The shift in the isotherm baseline (Fe Zr MOF MM is significantly lower than bidentate Zr UiO MOF across all pressures) confirms a reduction in available surface area due to the added mass and volume of the Fe complexes.

SI 8.3 BJH and NLDFT Analysis

Further to see how the addition of Iron (Fe) impacts the internal architecture, we analysed the BJH and NLDFT pore size distribution (PSD) data for parent bidentate Zr-UiO MOF and the Fe Zr MOF MM. The nitrogen adsorption–desorption isotherms and corresponding pore size distributions (PSDs) calculated via NLDFT and BJH methods for the bidentate Zr-UiO MOF and the Fe Zr MOF MM are provided in Figure S11.

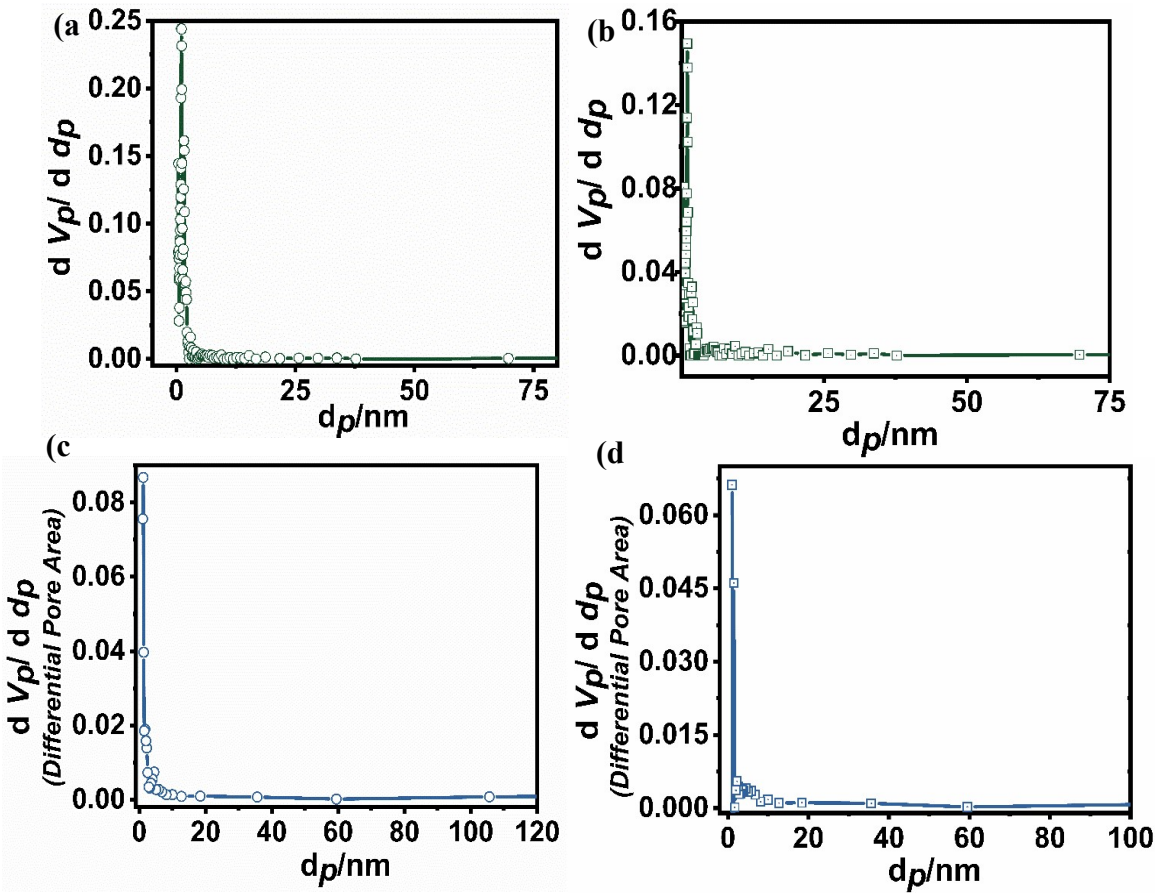

Figure S11 NLDFT analysis for bidentate Zr UiO MOF (b) NDLFT analysis of Fe Zr MOF MM (c) BJH analysis of bidentate Zr UiO MOF (d) BJH analysis of Fe Zr MOF MM

The NLDFT analysis reveals that the parent bidentate Zr UiO MOF possesses a dominant micropore population cantered at 1.58 nm with a micropore volume of 0.348 cm^3/g. Upon post-synthetic metalation with Fe to form Fe Zr MOF MM, the micropore volume significantly decreases to 0.224 cm^3/g (a reduction of approximately 35%). This substantial decrease in microporosity confirms that the Fe species are successfully coordinated to the pyridine groups of the bpydc linkers, which are located within the microporous tetrahedral and octahedral cages of the framework.

In contrast, the BJH analysis shows a much smaller reduction in mesopore volume, decreasing from 0.214 cm^3/g to 0.193 cm^3/g. The mesoporosity in these materials—often attributed to interparticle voids or framework defects—remains largely accessible.

Table S3: summarising the key changes w.r.t. the metric in both bidentate Zr UiO MOF and Fe Zr MOF MM respectively for NDLFT and BJH analysis.

S.No.	**Metric**	**Bidentate Zr UiO MOF**	**Fe Zr MOF MM**	**Key Change**
1.	NLDFT Peak (Micropore)	~1.58 nm	~1.14 nm	Shift/Reduction: Indicates Fe coordination inside cages.
2.	NLDFT Total Vol (V_p)	0.3480 cm^3/g	0.2241 cm^3/g	35% Decrease: Significant loss of micropore space.
3.	BJH Peak (Mesopore)	~1.19 nm	~1.04 nm	Minor shift in the low mesopore/pore-throat region.
4.	BJH Total Vol (V_p)	0.2142 cm^3/g	0.1935 cm^3/g	9% Decrease: Minimal impact on mesoporosity.

Therefore, it can be concluded that Fe loading predominantly affects the microporosity of the framework. The selective reduction in micropore volume compared to the relatively stable mesopore volume indicates that the metalation is site-specific to the linker's coordination sites within the framework's internal microporous environment, rather than a non-specific blockage of larger mesoporous channels.

SI 9 Post degradation Analysis (SEM & XRD Analysis)

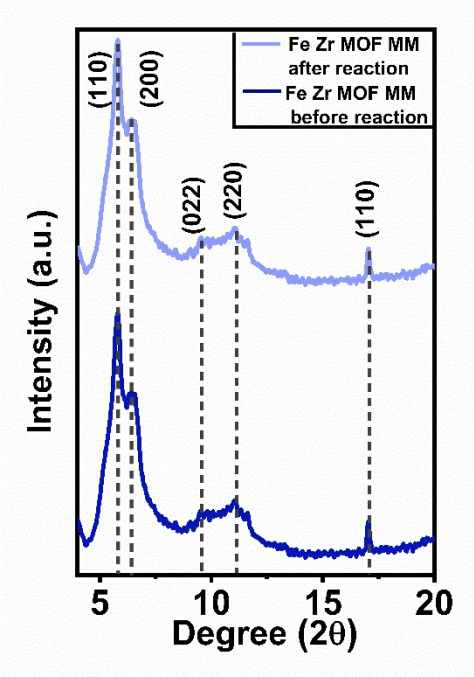

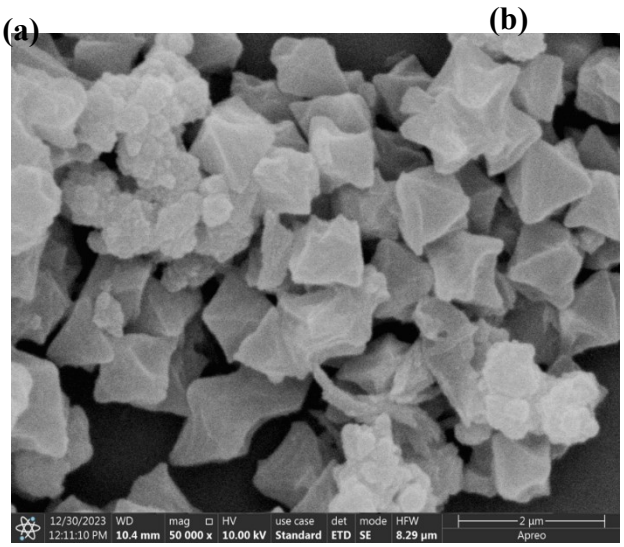

Figure S 12 (a) represents comparative XRD analysis of Fe Zr MOF MM before and after its interaction with amoxicillin antibiotic (b) FESEM analysis of Fe Zr MOF MM after it's interaction with amoxicillin antibiotic.

Figure S 12 (a) comparative XRD analysis of Fe Zr MOF MM before and after its interaction with amoxicillin antibiotic (b) FESEM analysis of Fe Zr MOF MM after it's interaction with amoxicillin antibiotic

Table S4: HRMS data as obtained from the graph with their respective predicted molecular formulas and their tentative structures, reported molecular weight from literature with their retention time

S.No.	Formula	Molecular weight received from HRMS data	Retention Time (mins)	Tentative structure
1.	$C_8H_{11}N_2O_4S$	229.13	10.2	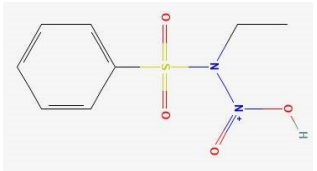
2.	$C_{14}H_{17}N_2O_2S$	274.27	12.23	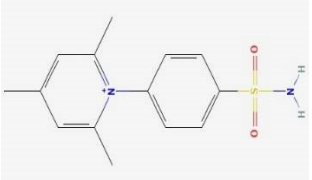

3.	$C_{15}H_{22}N_3O_4S$	349.08	7.01	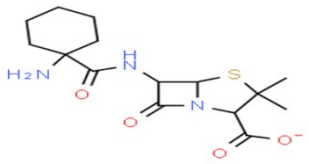
4.	**$C_{16}H_{19}N_3O_5NaS$**	**388.09**	**4.19**	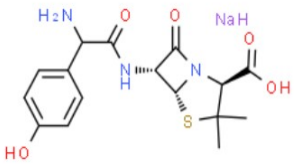
5.	$C_{16}H_{16}N_3O_8S$	410.07	11.89	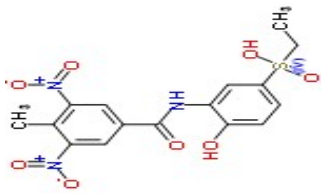
6.	$C_{16}H_{17}N_3O_8NaS$	437.19	15.86	

Leaching Studies: We performed Liquid Chromatography-Mass Spectrometry (LC-MS) analysis on the reaction solution after the removal of the Fe–Zr MOF MM. The LC-MS spectra primarily exhibited peaks corresponding to the transformation products and smaller intermediate fragments of amoxicillin degradation. Notably, no peaks associated with Fe-coordinated complexes or signals characteristic of metal-leached clusters were detected. While LC-MS is prioritized for organic intermediate identification, the absence of these signatures, combined with the maintained catalytic performance over multiple cycles, strongly suggests that the iron species remain integrally bound within the Zr6-based nodes. This indicates that the Fe–Zr MOF MM operates through a heterogeneous catalytic mechanism with negligible active-site leaching under the tested conditions.